Robotics and Autonomous Systems 172 (2024) 104586

Contents lists available at ScienceDirect

Robotics and Autonomous Systems

journal homepage: www.elsevier.com/locate/robot

# Assisted teleoperation control of robotic endoscope with visual feedback for nasotracheal intubation☆

Zhen Deng [a,b], Shengzhan Zhang [b], Yuxin Guo [b], Hongqi Jiang [b], Xiaochun Zheng [a,c,*], Bingwei He [b]

[a] Department of Anesthesiology, Shengli Clinical Medical College of Fujian Medical University, Fujian Provincial Hospital, Fuzhou, 350108, People's Republic of China

[b] Department of Mechanical Engineering and Automation, Fuzhou University, Fuzhou, 350108, People's Republic of China

[c] Fujian Emergency Medical Center, Fujian Provincial Key Laboratory of Emergency Medicine, Fujian Provincial Key Laboratory of Critical Medicine, Fujian Provincial Co-constructed Laboratory of "Belt and Road", Fuzhou, 350108, People's Republic of China

ARTICLE INFO

*Keywords:*
Surgical robotics
Robotic endoscope
Teleoperation control
Visual feedback assistance
Nasotracheal intubation

ABSTRACT

Endoscopic operation is one of the most difficult parts of nasotracheal intubation (NTI), a surgical procedure used to secure the airway of a patient. Due to the requirement of eye–hand coordination, manual operation of a flexible endoscope is challenging, even for an experienced surgeon. To enhance intubation efficiency, this paper developed a master–slave robotic nasotracheal intubation system (RNIS) for endoscopic operation. Movements in three degrees of freedom of the endoscope are controlled by the RNIS. An assisted teleoperation control strategy is designed to assist the operator in remotely controlling the pose, i.e., position and orientation, of the endoscope tip via a joystick. To ensure the efficiency of intubation, visual feedback assistance is hereby proposed, which fine-tunes the orientation of the endoscope tip as needed. The proposed system and methods are experimentally validated on a motion simulator and a phantom. The results demonstrated that the master–slave RNIS can successfully insert the flexible endoscope into the trachea of a phantom through the nasal cavity.

## 1. Introduction

Nasotracheal intubation (NTI) is one of the most popular surgical procedures to secure the airway of patients [1], where a surgeon needs to manually insert a flexible endoscope into the trachea of the patient through the nasal cavity (Fig. 1(A)). During the COVID-19 epidemic, NTI has been also used to establish artificial airways for patients [2]. To ensure proper intervention and visualization, the position and orientation of the endoscope tip need to be accurately adjusted as it travels along the human upper respiratory tract. Typically, the surgeon uses one hand to adjust the orientation of the endoscope tip and the other hand to control its feed motion. Consequently, endoscopic operation heavily relies on the hand–eye coordination ability of the surgeon, which is required through experience. Moreover, the unpredictable deformation of the flexible endoscope further complicates the endoscopic operation. Improper operations may cause serious surgical complications, such as epistaxis and perforation [3]. In this work, a master–slave robotic endoscopy system is proposed that is capable of operating the flexible endoscope during NTI.

To address the challenges of endoscopic operation, several robotic endoscopy systems have been introduced with their applications including laparoscopy [4], bronchoscopy [5], and colonoscopy [6]. However, a limited number of robotic systems have been proposed for the application of NTI [7,8]. Tighe et al. [9] performed the first robotically assisted endoscope intubation based on the Da Vinci surgical system. The operator remotely controlled the flexible endoscope via a master console. Although the system can steer the endoscope from the mouth into the trachea, the lumen center still relies on manual inspection. Moreover, the complexity and high cost of the Da Vinci surgical system have limited its medical applications. Hemmerling et al. [10,11] developed the Kepler Intubation System to control a video-laryngoscope rather than the flexible endoscope. The above two works based on commercial robots confirmed the feasibility of robotic

☆ This research was partly supported by the National Natural Science Foundation of China (No. 62003089), Fujian Provincial Health Technology Project, China (No. 2021ZD01003), and the Natural Science Foundation of Fujian Province, China (No. 2020J01455).

* Corresponding author at: Department of Anesthesiology, Shengli Clinical Medical College of Fujian Medical University, Fujian Provincial Hospital, Fuzhou, 350108, People's Republic of China.

*E-mail address:* zhengxiaochun7766@163.com (X. Zheng).

https://doi.org/10.1016/j.robot.2023.104586
Received 29 August 2022; Received in revised form 27 September 2023; Accepted 24 November 2023
Available online 28 November 2023

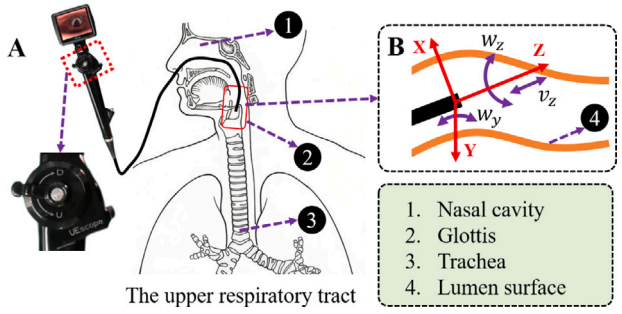


**Fig. 1.** Diagram of endoscopic operation in NTI. (A) An endoscope is controlled to travel along the human upper respiratory tract. The endoscope provides visualization to the operator. (B) The position and orientation of the endoscope tip are controlled to avoid collision with the lumen surface.

endoscopy. Boehler et al. [12] introduced a hand-held endoscopic device for tracheal intubation. However, the device can only adjust the orientation of the endoscope tip using visual feedback. The feeding motion of the endoscope requires manual operation. Moreover, holding the device by hand for a long time increases the physical burden on surgeons, leading to fatigue.

Several control strategies have been developed for robotic endoscopy [13], which are mainly categorized into two types, i.e., teleoperation control [14,15] and visual feedback control [16]. Under teleoperation control, robots are directly controlled by surgeons. Bajo et al. [14] performed the teleoperation of the robotic end-effector by defining a mapping between the slave end-effector and the master manipulator. Rozeboom et al. [17] demonstrated that teleoperation control can improve the intuitiveness and safety of surgical operations. Although teleoperation systems have been extensively used in various surgical robotic applications, most works adopt a master–slave paradigm, where the robot follows the command of the operator [18,19]. In this situation, the operator makes correct decisions and adjusts the position and orientation of the endoscope. On the other hand, visual feedback control refers to making corrective adjustments to the endoscope tip when visual feedback indicates that the state of the tip deviates from the desired state [20]. For example, Prendergast et al. [21] proposed a center tracking control algorithm based on visual feedback for robotic colonoscopy. However, ensuring the safety of surgery using visual feedback control is challenging, because the surgical environment is dynamic.

The orientation of the endoscope tip during NTI needs to be constantly adjusted so that it accurately tracks the lumen center without colliding with the lumen surface (Fig. 1(B)). Due to the spatial reasoning involved, remotely controlling the RNIS to orient the endoscope requires considerable time and effort. Several methods have been developed to improve the performance of teleoperation control [22–24]. Stap et al. [25] combined teleoperation control and visual servo control to steer a flexible endoscope in colonoscopy. However, the switch between the two control modes requires manual operation via a button. The robot cannot provide active assistance to the operator as needed. Li et al. [26] designed a role assignment law for human–robot shared control. Their work employs game theory with force feedback to coordinate the contribution between humans and robots during task execution. Girbes-Juan et al. [27] presented visual feedback assistance for dual-arm robot teleoperation in surface conditioning tasks. Their method was suitable for rigid robots rather than flexible endoscopes. Some works in the research of robot teleoperation used virtual fixtures to generate position or force signals to assist the operator in robot manipulation tasks [28,29]. For example, Lopez et al. [30] employed virtual fixtures to guide the operator towards the target anatomy during the teleoperation of a redundant surgical system. However, the virtual fixture was pre-designed pre-operatively without considering the changes in the intra-operative environment.

To achieve safe and effective endoscopic operation, this paper develops and validates a master–slave robotic nasotracheal intubation system (RNIS) for NTI. An assisted teleoperation control strategy is proposed, which maps the operator inputs to the RNIS to accomplish the adjustment of the endoscopic pose. The operator can remotely control the master–slave RNIS to steer a flexible endoscope to travel along the human upper respiratory tract. The effectiveness of the proposed method was demonstrated with real-world experiments. The contributions of this work can be summarized as follows:

- Development of the master–slave RNIS, including a robotic support arm, an endoscope steering unit, a flexible endoscope, and a joystick. The mechanism design of the RNIS can meet the requirement of motion control of the flexible endoscopy. The three degrees of freedom (DOF) movement of the endoscope is controlled to allow insertion into the trachea through the nasal cavity.
- An assisted teleoperation control strategy is proposed for the RNIS to adjust the pose of the endoscope tip. Visual feedback assistance is considered to fine-tune the orientation of the endoscope tip as needed, reducing the burden on the operator. The proposed role assignment strategy allows human–robot coordination during intubation.
- Extensive experiments on based a motion simulator and a phantom are carried out to demonstrate the feasibility of the proposed master–slave RNIS and the effectiveness of the proposed control strategy.

The remainder of this paper is organized as follows. The design of the master–slave RNIS specified for the NTI is introduced in Section 2. The assisted teleoperation control strategy for steering the flexible endoscope and its core components are presented in Section 3. In Section 4, two kinds of experiments and methods performed to validate the proposed system are described. The experimental results are shown and discussed. Finally, Section 5 concludes this work.

## 2. Development of Master–slave robotic nasotracheal intubation system

This section introduces the design of the master–slave RNIS, which comprises four modules, namely a robotic support arm (RSA), an endoscope steering unit (ESU), a flexible endoscope, and a joystick (Logitech Extreme 3D Pro), as shown in Fig. 2.

The RSA enables global positioning of endoscopes close to the patient's nasal cavity (Fig. 2(B)). It has a four-DOF Prismatic-Revolute-Revolute-Revolute-type (PRRR) configuration. The first joint of the RAS is the prismatic joint and the other three joints are the rotation joints that adjust the orientation of the ESU. These rotation joints are locked by means of nuts. By loosening the nut, the operator can manually drag the RSA to position the endoscope. Tightening the nut allows the RSA to act as a support.

The endoscope end has three degrees of freedom, i.e., rotation motion $w_z$, bending motion $w_y$, and feed motion $v_z$, as shown in Fig. 1(B). Based on the motion analysis of the endoscope, the ESU is designed to have five motors (Fig. 2(C)). The motor (*M1*) controls the rotation of the endoscope around its axis, thus realizing the rotational motion $w_z$ of the endoscope tip. The motor *M2* controls the bending motion $w_y$ of the endoscope tip by rotating the knob on the endoscope handle. The motor (*M3*) at the proximal end is used to steer the feeding motion $v_z$ of the endoscope. Straightening and clamping of the endoscope is based on motors 4 and 5.

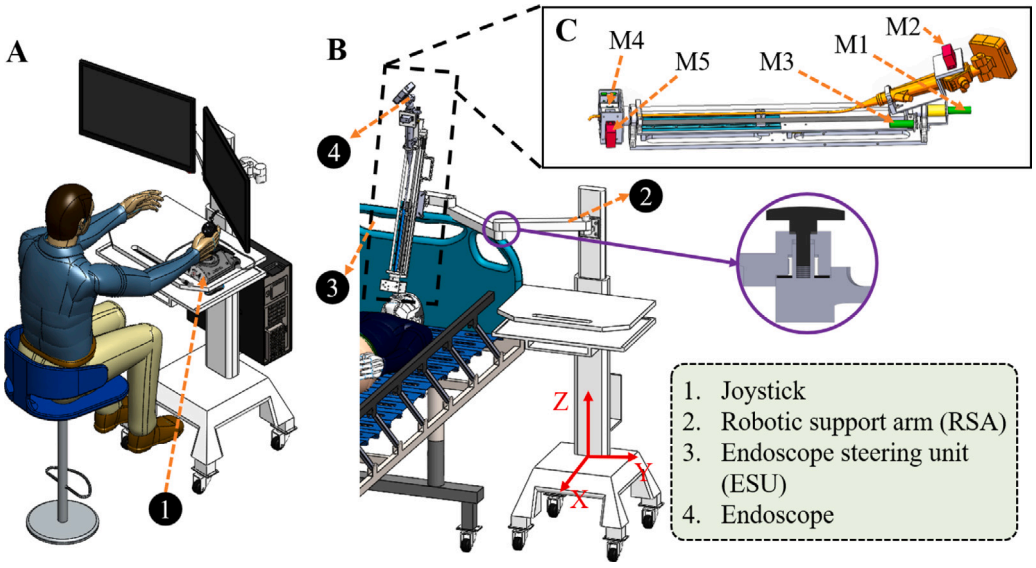


**Fig. 2.** Overview of the proposed master–slave RNIS. (A) An operator remotely controls the RNIS via a joystick while observing endoscopic images. (B) The RNIS steers the endoscope to travel along the upper respiratory tract of a patient. (C) The structure of the ESU.

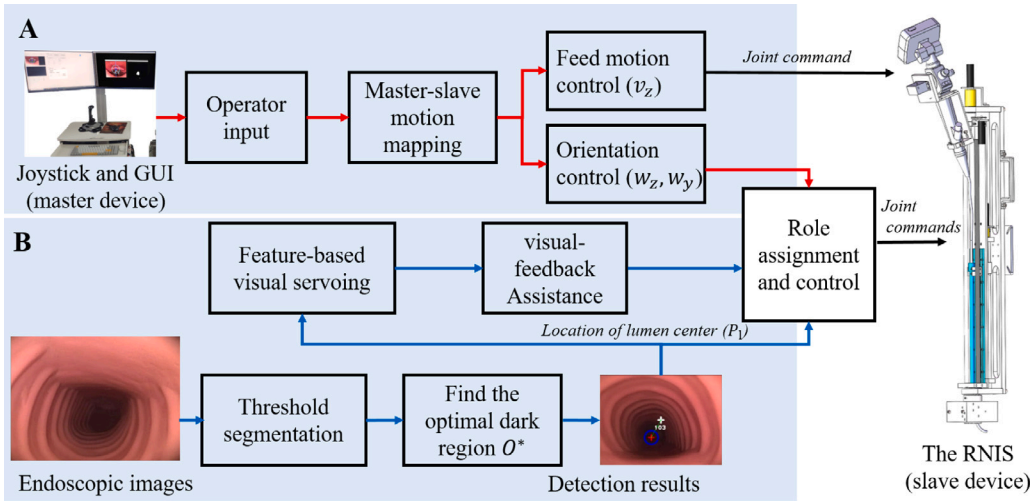


**Fig. 3.** Assisted teleoperation control strategy of the master–slave RNIS. (A) Full teleoperation by the operator, (B) Visual-feedback assistance with lumen center detection. The location of the lumen center is detected as the desired moving target of the endoscope tip.

## 3. Assisted teleoperation control

This section presents the assisted teleoperation control strategy for the master–slave RNIS to steer the flexible endoscope (Fig. 3). Teleoperation control is performed by establishing a mapping between the operation of the joystick and the adjustment of the endoscope tip. Then, visual feedback control is employed to generate assistance for the operator to fine-tune the orientation of the endoscope tip, where a lumen center detection method is designed to determine the location of the lumen center in the image. A role assignment law is designed to coordinate the contribution of visual feedback assistance during the orientation control of the endoscope tip.

### 3.1. Master–slave motion mapping

The motion mapping between the operation of the joystick and the adjustment of the endoscope tip for the teleoperation of the RNIS is hereby defined as in Fig. 4. The putter and throttle of the joystick are used to generate the operator input, which is further mapped to the adjustment of the endoscope tip. As shown in Fig. 4 The roller control button is used to open and close the rollers. the Deadman button is set to ensure the safety of endoscopic operation. Pressing the Deadman button stops the RNIS immediately and keeps still holding the endoscope.

To intuitively adjust the orientation of the endoscope tip, the motion of the joystick is first mapped to the motion velocity of the image center in the image frame and then mapped to the orientation adjustment of the endoscope tip. In this way, the operator only needs to pay attention to the image changes without considering the robot state. During intubation, the endoscope is teleoperated by the operator to decrease the error between the $P_c$ and the lumen center $P_l$. A 2-D cross defined on the putter of the joystick describes the two operator inputs ($f_1$ and $f_2$) (Fig. 4). An image frame is also defined on the image with its origin at the image center $P_c$. Therefore, the operator input $F_{12} = [f_1, f_2]^T$ from the joystick is mapped to the motion velocity $V_c = [v_{cx}, v_{cy}]^T$ of the $P_c$, respectively (see corresponding frames in Fig. 4). This work defines a linear transformation to map both velocities

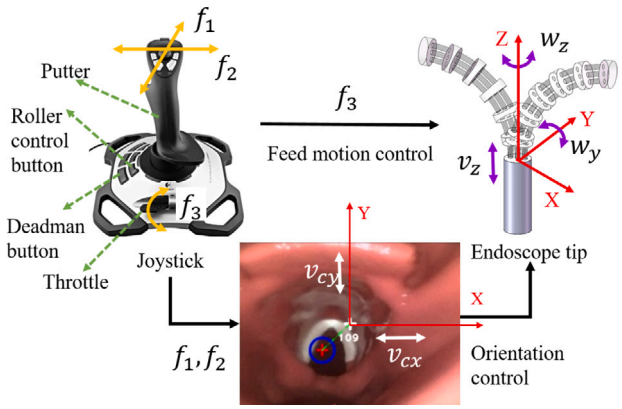


**Fig. 4.** Schematic diagram of the master–slave motion mapping between the operator input and the endoscope tip.

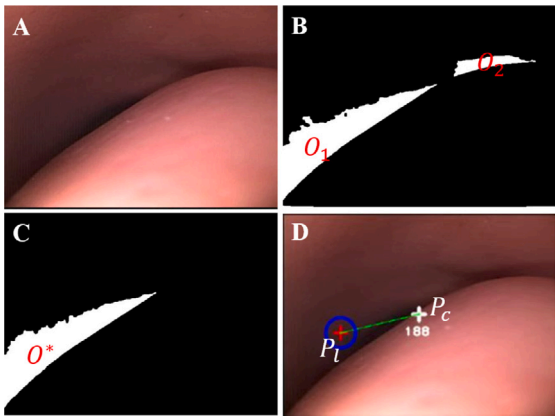


**Fig. 5.** Example of lumen center detection. (A) the original image. (B) The result of threshold segmentation. $O_1$ and $O_2$ are the two segmented regions. (C) the optimal dark region $O^*$. (D) the final result of lumen center detection. The lumen center (red cross) and the image center (white cross) are displayed.

for orientation control as

$$v_{cx} = \begin{cases} v^{cx}_{\max}, & f_1 \geq \delta^x_{\max} \\ -v^{cx}_{\max}, & f_1 \leq -\delta^x_{\max} \\ 0, & |f_1| \leq \delta^x_{\min} \\ k_{x,1} f_1, & Otherwise \end{cases} \tag{1}$$

$$v_{cy} = \begin{cases} v^{cy}_{\max}, & f_2 \geq \delta^y_{\max} \\ -v^{cy}_{\max}, & f_2 \leq -\delta^y_{\max} \\ 0, & |f_2| \leq \delta^y_{\min} \\ k_{y,1} f_2, & Otherwise \end{cases} \tag{2}$$

where $K_1 = [k_{x,1}, k_{y,1}]^T$ denote two constant scaling factors for the mapping from $F_{12}$ to $V_c$. ($\delta^x_{\max}$, $\delta^x_{\min}$) and ($\delta^y_{\max}$, $\delta^y_{\min}$) represents thresholds for maximum and minimum inputs, respectively. When the absolute value of $f_1$ or $f_2$ is less than the minimum thresholds (i.e., $\delta^x_{\min}$ and $\delta^y_{\min}$), the orientation of the endoscope tip remains stationary, thus reducing the influence of the operator's handshaking. Then, the motion velocity $V_c = [v_{cx}, v_{cy}]^T$ of the $P_c$ the image space is mapped to the orientation adjustment $W'_e = [w'_y, w'_z]^T$ of the endoscope tip (see corresponding frames in Fig. 4). This work defines a task Jacobean to map both velocities for orientation control as

$$W'_e = J \cdot K_2 \cdot V_c \tag{3}$$

with

$$K_2 = \begin{bmatrix} k_{x2} & 0 \\ 0 & k_{y2} \end{bmatrix}$$

where $K_2$ is a constant scaling matrix. $J$ is the Jacobian matrix defined in task space, which decouples the rotation and bending motion of the endoscope tip. $\theta$ denotes the rotation angle of the tip frame of the endoscope with respect to the image frame in the plane. In this way, the operator input $F_{12}$ is indirectly mapped to the orientation adjustment $W'_e$ of the endoscope tip.

$$J = \begin{bmatrix} cos(\theta) & sin(\theta) \\ -sin(\theta) & cos(\theta) \end{bmatrix} \tag{4}$$

The operator remotely controls the feed velocity of the endoscope tip via the throttle of the joystick (Fig. 4). The input $f_3$ is mapped to the feeding velocity $v_z$ of the endoscope through a linear transformation as follows.

$$v_z = \begin{cases} v^z_{\max}, & f_3 \geq \delta^z_{\max} \\ -v^z_{\max}, & f_3 \leq -\delta^z_{\max} \\ 0, & |f_3| \leq \delta^z_{\min} \\ k_z f_3, & Otherwise \end{cases} \tag{5}$$

where $k_z$ is a constant scaling factor for the mapping from $f_3$ to $v_z$. As a result, movement in three DOF of the endoscope, i.e., feed motion $v_z$, rotation motion $w_z$, and bending motion $w_y$, is remotely controlled by the human operator via a joystick.

### 3.2. Visual-feedback assistance

Controlling the orientation of the endoscope tip is not intuitive, since it requires spatial reasoning. Confusion from the surgeon in terms of tracking the desired target is often the case in NTI. To address this issue, this work proposes visual feedback assistance to compensate for the orientation error of the endoscope tip. In the following, the implementation of visual feedback assistance is described.

The lumen center $P_l$ is detected as the desired moving target of the endoscope tip. Following the assumption that the center of the darkest region in the image is the location of the lumen center [31,32], this work detects the lumen center by segmenting dark regions in the image. First, the RBG image (Fig. 5(A)) captured by the endoscope is converted to an 8-bit gray-scale image $I(x, y)$. To enhance image contrast, a histogram equalization operator is employed to generate the image $I'(x, y)$. Then, an adaptive threshold algorithm is applied to binaries $I'(x, y)$, and generate a new image $I''(x, y)$. The regions with relatively low light intensity are segmented from $I''(x, y)$ (Fig. 5(B)). Finally, a criterion to filter out unreasonable regions and determine the optimal dark region $O^*$ is defined as follows

$$O^* = \max_{j \in i,2,\ldots,n} C(O_j) \quad with \quad C = \frac{A^2}{\sqrt{l_{\min} l_{mean}}} \tag{6}$$

where $O_j$ denote one of the segmented regions. $A$ represents the area of the segmented region $O_j$. $l_{\min}$ and $l_{mean}$ represent the minimum and mean gray values of pixels in the region $O_j$, respectively.

Once the optimal dark region $O^*$ is filtered (Fig. 5(C)), the center $C_o = [c^o_x, c^o_y]$ of $O^*$ is computed in Eq. (7), which is taken as the location of the lumen center $P_l = [p_{lx}, p_{ly}]$.

$$C_o = \begin{bmatrix} c^o_x \\ c^o_y \end{bmatrix} = \frac{\sum_{(x,y) \in O^*} \begin{bmatrix} x \\ y \end{bmatrix} I''(x, y)}{\sum_{(x,y) \in O^*} I''(x, y)} \tag{7}$$

To accurately track the lumen center, this employs a proportional–derivative controller [33] to fine-tune the orientation of the endoscope tip. The control error is defined as $e_p = p_l - p_c$. The output of the controller is the rotation and bending velocities of the endoscope, i.e., $W''_e = [w''_y, w''_z]^T$.

$$W''_e = K_p e_p(t) + K_d \frac{de_p}{dt}(t) \tag{8}$$

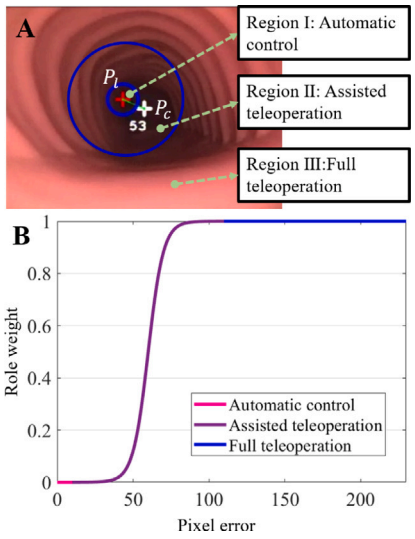


**Fig. 6.** Definition of the role assignment law. (A) Division of three control regions in the image. The error $E_p$ between $P_l$ and $P_c$ is 53. (B) Assigning different role weights according to different control areas.

with

$$K_p = \begin{bmatrix} k_{px} & 0 \\ 0 & k_{py} \end{bmatrix} \quad K_d = \begin{bmatrix} k_{dx} & 0 \\ 0 & k_{dy} \end{bmatrix}$$

where $K_p$ and $K_d$ denote the proportional and derivative parameters of the controller, respectively. In this way, the visual feedback controller provides assistance to the operator. The endoscope tip is adjusted towards the lumen center for smooth progression along the upper respiratory tract.

### 3.3. Role assignment

A role assignment law is proposed to coordinate the contribution of visual feedback assistance during the teleoperation of the RNIS. The operator can receive assistance on the orientation control of the endoscope tip as needed. In this work, when $P_l$ is far from $P_c$, the operator takes the lead role to control the RNIS, quickly eliminating the large error $E_p$ via the joystick. On the other hand, once the endoscope tip is near $P_l$, the contribution of the assistance provided by the RNIS is improved, because the RNIS can control the orientation of the endoscope tip more precisely under a small error.

The contribution of visual-feedback assistance is adapted through a role weight, which is computed based on the error $E_p$ in the image space (Fig. 6(A)). Based on the error $E_p$, the image space is divided into three regions, i.e., Region I: Automatic control ($E_p \leq E_{p,\min}$), Region II: Assisted teleoperation ($E_{p,\min} < E_p < E_{p,\max}$), and Region III: Full teleoperation ($E_p \geq E_{p,\max}$). Then, the corresponding role weight is computed as Eq. (9). Different from [25], the role weight is continuous and not a discrete switching between different states.

$$\alpha = \begin{cases} 1, & E_p \geq E_{p,\max} \\ sigmoid(E_p), & E_{p,\min} < E_p < E_{p,\max} \\ 0, & E_p \leq E_{p,\min} \end{cases} \tag{9}$$

with

$$E_p = \sqrt{(p_{lx} - p_{cx})^2 + (p_{ly} - p_{cy})^2}$$

when $P_l$ located in Region II, the operator remotely controls the position and orientation of the endoscope tip via the joystick, while the visual-feedback assistance provided by the RNIS is used to fine-tune its orientation. Teleoperation with assistance can improve control accuracy and reduce the burden on the operator. When $P_l$ is located in Region III, the RNIS only considers the command from the joystick. Finally, when $P_l$ is located in Region I, the endoscope tip is close enough to the desired target direction. Visual-feedback assistance fine-tunes the orientation of the endoscope tip and the teleoperation command is ignored to avoid the impact of the operator's handshaking.

As a consequence, the final control command for the orientation control of the endoscope tip is computed as follows

$$W_e = \alpha W_e' + (1 - \alpha) W_e'' \tag{10}$$

where $W_e = [w_y, w_z]^T$ are the rotation and bending velocities of the endoscope tip generated by the proposed assisted teleoperation control method. When the endoscope tip is near the lumen center, the visual feedback assistance is considered, otherwise, only teleoperation control is carried out. The implementation details of the proposed assisted teleoperation control for the master–slave RNIS are summarized in Algorithm 1.

**Algorithm 1:** Assisted teleoperation control of the RNIS

**Input:** Distance threshold ($E_{p,min}$, $E_{p,max}$)
Using endoscope to capture image $I(x, y)$ ;
**while** *endoscope tip doesn't reach the trachea* **do**
  $I''(x, y) \leftarrow$ perform adaptive threshold segmentation ;
  $O^* \leftarrow$ filter dark regions $O_j$ in $I''(x, y)$ ;
  $P_l = (p_{lx}, p_{ly}) \leftarrow$ detect the lumen center ;
  $E_p \leftarrow$ compute the error between $P_l$ and $P_c$ ;
  $F_{12}$ and $f_3 \leftarrow$ recorded from the joystick ;
  $W_e' = [w_y', w_z']^T$ and $v_z \leftarrow$ motion mapping from $F_{12}$ and $f_3$ ;
  **if** $E_p < E_{p,max}$ **then**
    $\alpha \leftarrow$ compute role weight based on $E_p$ ;
    $W_e'' = [w_y'', w_z'']^T \leftarrow$ Visual feedback control ;
    update $W_e = \alpha W_e' + (1 - \alpha) W_e''$ ;
  **else**
    update $W_e = W_e'$ ;
  **end**
  Motor control of the RNIS with $W_e = [w_y, w_z]^T$ and $v_z$;
**end**

## 4. Experiments

Experiments were performed to evaluate the performance of the master–slave RNIS and the proposed control strategy. First, the performance of the proposed method was systematically described using target-tracking tasks based on a motion simulator. Then, the effectiveness of the proposed RNIS system was further validated on a phantom.

### 4.1. Experiment with a motion simulator

#### 4.1.1. Experimental setups

The target tracking task was assigned to the master–slave RNIS in this experiment. Fig. 7 shows the experimental setup. A two-DOF motion simulator was developed, which allowed a black spot on the white plane to move in the plane. The motion simulator was actuated by two stepper motors. The workspace of the moving spot was 100 mm× 10 mm in the plane. The flexible endoscope was remotely controlled by the operator to track the moving spot, which simulated the movement of the lumen center in the human upper respiratory tract. Images with a resolution of 640*480 pixels were captured by a monocular camera at the endoscope tip.

The motion trajectory of the spot was set to be an "I" shape, which comprised nine segments (Fig. 8(B)). The black spot was controlled to move through the nine piece-wise trajectories in turn, i.e., from ① to ⑨. During robot teleoperation, the location of the spot in the image space was detected and displayed to the operator. The orientation of the endoscope tip is then adjusted by the RNIS to reduce the error $E_p$

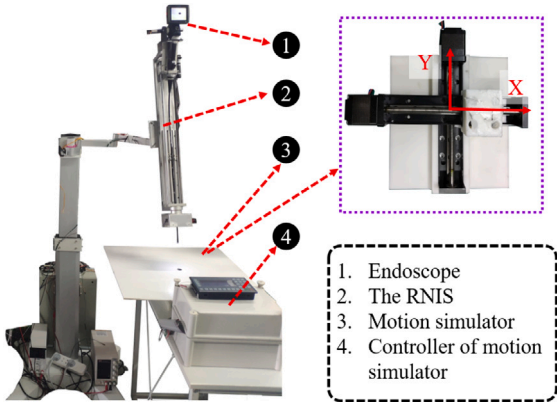


**Fig. 7.** Setup of the experimental platform based on a motion simulator. The overhead view of the motion simulator is shown on the right top.

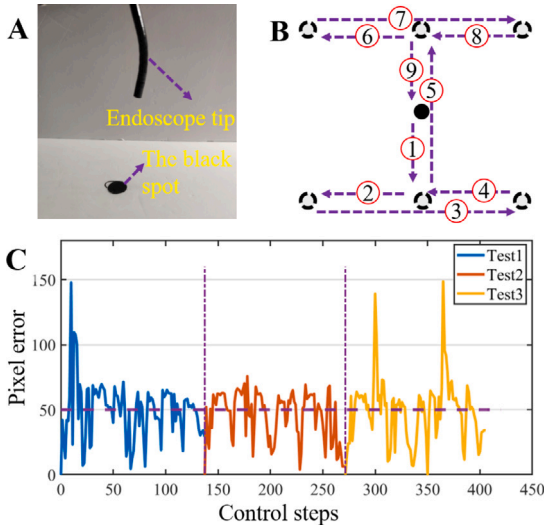


**Fig. 8.** Experimental results of the RNIS for tracking a moving target on the motion simulator. (A) A snapshot of the endoscope tip during target tracking. (B) The planned motion trajectory of the moving spot, from ① to ⑨. (C) The error during the visual tracking in three tests.

between the spot and the image center $P_c = (320, 240)$. When the error $E_p$ was less than 50 pixels, the endoscope tip was considered to reach the target.

#### 4.1.2. Validation of the assisted teleoperation method

Fig. 8 shows the results of the RNIS for tracking the moving target. The motion velocity of the spot was set to be 5 mm/s in this experiment. The error $E_p$ was measured as an evaluation metric. From Fig. 8(C), the endoscope tracked the moving spot accurately, since the error was relatively low. Here, the motion range of the pot was $0 \sim 320$ pixels in the X direction and $0 \sim 240$ pixels in the Y direction. It can be seen that the spot approached in the image center, and remains near the target region (i.e., the error remained under 50 pixels). The orientation of the endoscope can be effectively adjusted by the RNIS using teleoperation control to track the moving target.

A certain fluctuation of the error was observed during the tracking process. There are two main reasons for the sudden increase in tracking error: (1) The direction of movement of the moving spot changed suddenly and the operator did not respond in time. (2) The experiments are subject to external lighting conditions, which make erroneous detection of moving target points. However, it is worth noting that throughout the experiment, only a few frames showed recognition

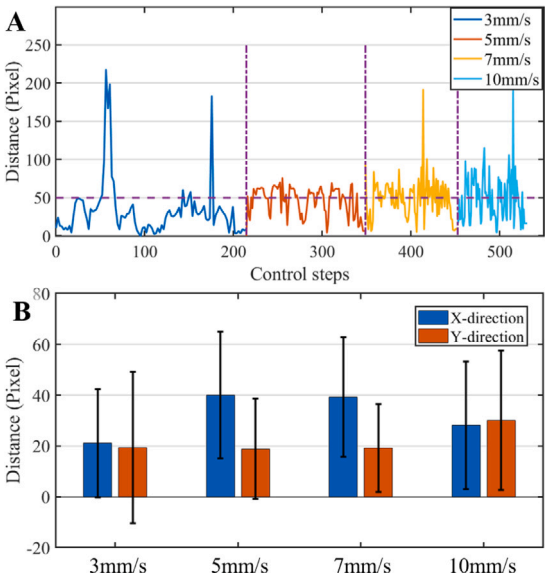


**Fig. 9.** Experimental results of moving target tracking under different velocity conditions. (A) The errors of the proposed teleoperation control strategy for tracking a target at different velocities. (B) The mean and variance of the errors in the X and Y directions of the image space.

errors, which did not affect the overall control performance. In clinical NTI, sudden changes in the location of the lumen center may occur due to changes in the patient's posture or drug stimulation. The result indicates that once the moving spot is away from the image center, the operator remotely controls the RNIS to quickly reduce the error. The proposed teleoperation control method achieved a good target tracking performance.

#### 4.1.3. Experiments at different moving velocities

In clinical NTI, the surgeon steers the endoscope into the upper respiratory tract at different velocities. Accordingly, the location of the lumen center changes at different velocities. For this reason, additional experiments were performed to evaluate the target tracking performance under different velocity conditions. Four motion velocities (i.e., 3, 5, 7, and 10 mm/s) of the spot were tested. Ten trials were performed for each velocity, in which the spot followed the same trajectory as in the above experiment.

Fig. 9 shows the result of all 40 experiments. The error is relatively low among all four velocities (Fig. 9(A)). In the case of 3 mm/s, there are two sudden increases in the error. This is due to the operator's misoperation resulting in an excessive amount of control. On the other hand, The increase in endoscopic movement velocity can reduce the operation time but may reduce the stability of endoscopic operation. As we can see from Fig. 9 (B), the fluctuation degree of the error at 10mm/s is higher than the other three velocities. Therefore, while controlling the orientation of the endoscope, the operator also needs to reasonably control the feeding velocity of the endoscope to avoid sudden high-speed feeding. This comparative experiment demonstrated that the RNIS with the proposed teleoperation method works well in tracking the target moving at different velocities.

#### 4.1.4. Validation of visual-feedback assistance

To evaluate the effectiveness of the proposed visual feedback assistance, an additional experiment was performed. In the literature of robotic shared control, the linear and tangent functions have been widely used to calculate the role weight [22], which is compared in this work to assess the performance of the role assignment law. Therefore, four sets of experiments were carried out:

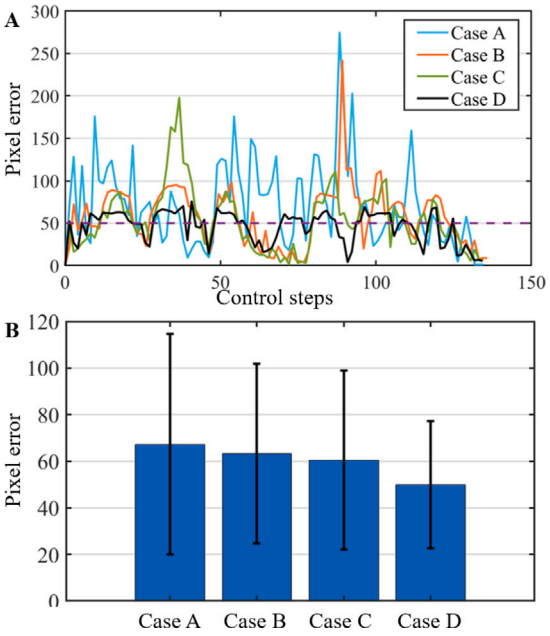


**Fig. 10.** Experimental results of teleoperation control strategies. (A) The errors of the four cases. (B) The mean and standard deviation of the errors in the image space.

- Case A (Unassisted teleoperation): The operator remotely controlled the RNIS without assistance;
- Case B(Assisted teleoperation with linear weight): The role weight was defined based on a linear function;
- Case C (Assisted teleoperation with tangent weight): The role weight was computed based on a tangent function;
- Case D (Proposed Assisted teleoperation method): The endoscope was teleoperated with visual feedback assistance.

The setups of this comparative experiment were the same as the above experiment. Fig. 10 shows the result of the four sets of experiments. Fig. 10(A) shows that there is a fluctuation of the error in Case A, meaning that the movement of the endoscope tip in Case A was unstable. In addition, the results also show that the operator is prone to misoperation in Case A, resulting in a sudden increase in the error sometimes. However, in Case D, the fluctuation of the error is minimal, which means that the endoscope tip can steadily track the lumen center. Visual feedback assistance helped the operator improve the stability and accuracy of endoscopic control. Fig. 10(B) shows that the mean and standard deviation of the error in Case B and C are higher than the corresponding results of Case D. This is because the sigmoid function can calculate the role weights of RNIS and operators more efficiently, making role switching more natural. Thus, the results demonstrated that visual feedback assistance works well together with the role assignment law.

### 4.2. Experiment on a phantom

#### 4.2.1. Experimental setup

The effectiveness of the proposed system and method was further validated based on a phantom (Fig. 11). In this experiment, the operator remotely controlled the RNIS via a joystick to insert the endoscope into the upper respiratory tract of the phantom. Endoscopic images were displayed on a computer screen. The robot control software was implemented in C++ and runs on a standard Windows computer (2.50 GHz Intel i9 CPU). Table 1 shows the parameter setting for assisted teleoperation control of the endoscope.

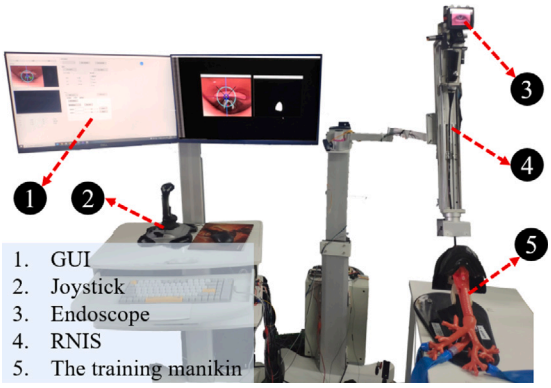


**Fig. 11.** Experimental setup based on a phantom.

**Table 1**
The parameter setting for assisted teleoperation control of the endoscope.

| Parameter | Value |
|---|---|
| $K_1 = [k_{x,1}, k_{y,1}]^T$ | [5.0, 0.1] |
| $K_2 = [k_{x,2}, k_{y,2}]^T$ | [740, 54] |
| $k_z$ | 4.0 |
| $(\delta^x_{max}, \delta^x_{min})$ | (950, 300) |
| $(\delta^y_{max}, \delta^y_{min})$ | (950, 450) |
| $(k_{x,p}, k_{x,d})$ | (30, 5) |
| $(k_{y,p}, k_{y,d})$ | (0.5, 0.1) |
| $(E_{p,max}, E_{p,min})$ | (110, 10) |

A user study was performed to validate the effectiveness of the proposed RNIS. Nine expert anesthesiologists from Fujian Provincial Hospital were recruited as the participants. Therefore, three groups of experiments were performed:

- Group A (Manual operation): three of the nine experts manually controlled the endoscope on the phantom following clinical procedures;
- Group B (Unassisted teleoperation): the other three experts teleoperated with the RNIS to operate the endoscope without assistance.
- Group C (Assisted teleoperation): three of the nine experts teleoperated the RNIS to operate the endoscope with visual feedback assistance;

Three evaluation metrics were employed in this experiment as follows: 1) The error ($E_p$): the distance between the $P_l$ and the $P_c$; 2) Number of collisions ($N_m$): When the lumen center is out of view, the endoscope is considered to collide with the lumen surface, and 3)Operation time ($T_m$): the time required for the endoscope to travel from the nasal cavity to the trachea.

#### 4.2.2. Results and discussion

Fig. 12 shows the result of the three groups of experiments. Fig. 12(a) shows the errors ($E_p$) of the three groups of experiments. The average error in Group C was about 55 pixels, which is lower than in Group A. This indicates that compared with manual operation, the RNIS tracked the lumen center more accurately. In Groups B and C, the movement of the endoscope along the upper respiratory tract is more smooth. In addition, compared with Group B, the average error in Group A was reduced by about 30%, when considering visual-feedback assistance during robot teleoperation. The result demonstrates that the visual-feedback assistance enables the RNIS to track the lumen center more accurately.

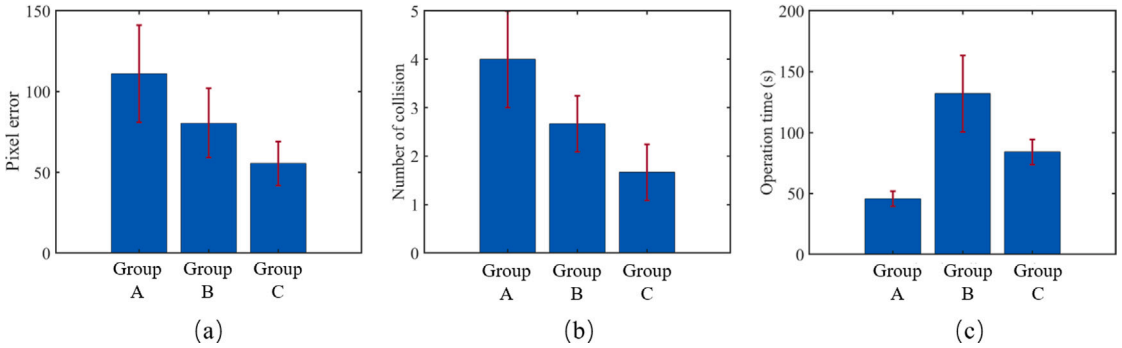


**Fig. 12.** Experimental results of the RNIS for endoscope operation on a phantom. (A) The error between the lumen center and the image center. (B) Number of collisions between the endoscope tip and the lumen surface. (D) The operation time for the endoscope to travel from the nasal cavity to the trachea.

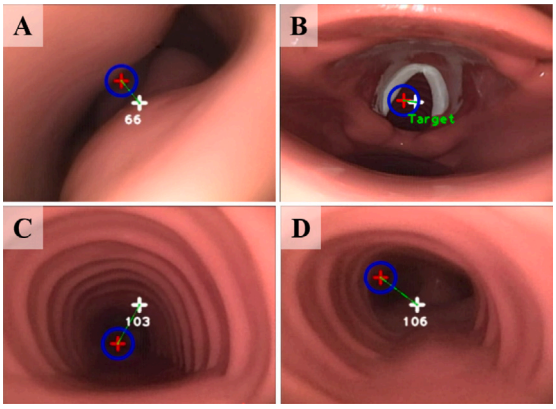


**Fig. 13.** Snapshots of assisted teleoperation control of the RNIS during performing intubation intervention in NTI. The endoscope passes through different anatomical structures, namely (A) the nasal cavity. (B) the glottis. (C) the trachea. (D) The tracheal carina.

During the teleoperation of the RNIS, the collision between the endoscope tip and the lumen surface should be avoided for the safety of the operation. Fig. 12(b) shows the number of collisions ($N_m$) from the three groups of experiments. Compared with Groups B and C, the endoscope tip is more prone to collide with the lumen surface in Group A. Excessive collisions in Group A indicate that the movement of the endoscope is unstable. The main reason is that during manual operation, the participants tended to drastically adjust the endoscope to complete the intubation operation, which increased the probability of collision. Group C had the least collisions, 42% less than Group A. In the teleoperation control mode, the operator adjusts the endoscope finely according to image feedback, thus achieving smooth movement of the endoscope.

Operation time ($T_m$) is another important metric, because the prolonged endoscopy operation may lead to hypoxia. The average operation time in Group A was shorter than that in Groups B and C (Fig. 12(c)). The participants are more familiar with the operation of endoscopes than the RNIS, thus manual operation can be faster. The operation time of Group C was about 80 s, which is in accordance with the surgical requirements. In addition, the mean and standard deviation of the operation time in Group C was larger than that of Group B, considering visual feedback assistance led to a decreased time in the intubation when the operator remotely controlled the RNIS via the joystick. Thus, the results demonstrated that the proposed RNIS is able to insert a flexible endoscope into the trachea through the nasal cavity within an appropriate time frame.

The movement of the endoscope along the upper respiratory tract was analyzed as demonstrated in Fig. 13. During intubation, the endoscope passes through the nasal cavity, glottis, and trachea until it reaches the trachea carina. The red cross in the images denotes the location of the lumen center generated by the proposed detection method, and the white cross represents the location of the image center, which is taken as the desired moving target of the endoscope tip. The number denotes the value of the error $E_p$. Experiments demonstrated the RNIS can successfully steer the flexible endoscope to travel along the upper respiratory tract. It is worth noting that the endoscope demanded longer (about 15 seconds) to pass through the glottis. This is due to the relatively more complex anatomy and the smaller workspace in the glottis section. The orientation of the endoscope needs to be accurately adjusted before it passes through the glottis smoothly. In future work, we plan to combine a dynamic virtual fixture with the control strategy, especially at the glottis, to further improve intubation efficiency,

## 5. Conclusion

A master–slave robotic nasotracheal intubation system (RNIS) for endoscopic operation in nasotracheal intubation (NTI) was presented in this paper and the proposed assisted teleoperation method was further validated. Due to the requirement of eye–hand coordination, manual operation of the flexible endoscope is challenging. Using the developed RNIS, the operator can remotely steer the endoscope to travel along the upper respiratory tract. A teleoperation control method was designed by establishing the correspondence between the operation of the joystick and the response of the endoscope. In addition, visual feedback assistance was integrated into the teleoperation control strategy to fine-tune the orientation of the endoscope tip, thereby improving the stability and accuracy of endoscopic control. Finally, experiments performed on the motion simulator demonstrated that based on the proposed methods, the master–slave RNIS performed well in the orientation control of the flexible endoscope. The experiments on the phantom demonstrated the effectiveness of the proposed system and methods in operating endoscopes during NTI.

Future work will focus on the integration of more realistic factors, for example, the opening and closing motion of the glottis during surgery. For clinical applications, animal experiments should be performed to optimize and validate the master–slave RNIS.

## Declaration of competing interest

The authors declare that they have no known competing financial interests or personal relationships that could have appeared to influence the work reported in this paper.

## Data availability

Data will be made available on request.

## References


[1] D. Prasanna, S. Bhat, Nasotracheal intubation: An overview, J. Maxillofacial Oral Surg. 13 (4) (2014) 366–372.

[2] A. Zemmar, A.M. Lozano, B.J. Nelson, The rise of robots in surgical environments during COVID-19, Nat. Mach. Intell. 2 (10) (2020) 566–572.

[3] M. Tsukamoto, T. Hitosugi, T. Yokoyama, Awake fiberoptic nasotracheal intubation for patients with difficult airway, J. Dent. Anesthesia Pain Med. 18 (5) (2018) 301–304.

[4] K. Xu, J. Zhao, M. Fu, Development of the SJTU unfoldable robotic system (SURS) for single port laparoscopy, IEEE/ASME Trans. Mechatronics 20 (5) (2014) 2133–2145.

[5] A.J. Kent, K.A. Byrnes, S.H. Chang, State of the art: Robotic bronchoscopy, in: Seminars in Thoracic and Cardiovascular Surgery, Elsevier.

[6] J.W. Martin, B. Scaglioni, J.C. Norton, V. Subramanian, A. Arezzo, K.L. Obstein, P. Valdastri, Enabling the future of colonoscopy with intelligent and autonomous magnetic manipulation, Nat. Mach. Intell. 2 (10) (2020) 595–606.

[7] Z. Slavković, D.M. Stamenković, P. Romić, A. Tomić, N. Milović, M. Jovanović, M. Karanikolas, The present and future of fiberoptic intubation, Vojnosanitetski Pregled 70 (1) (2013) 61–67.

[8] B.S. Peters, P.R. Armijo, C. Krause, S.A. Choudhury, D. Oleynikov, Review of emerging surgical robotic technology, Surg. Endosc. 32 (4) (2018) 1636–1655.

[9] P.J. Tighe, S. Badiyan, I. Luria, S. Lampotang, S. Parekattil, Robot-assisted airway support: A simulated case, Anesthesia Analgesia 111 (4) (2010) 929.

[10] T. Hemmerling, R. Taddei, M. Wehbe, C. Zaouter, S. Cyr, J. Morse, First robotic tracheal intubations in humans using the Kepler intubation system, Br. J. Anaesthesia 108 (6) (2012) 1011–1016.

[11] T.M. Hemmerling, M. Wehbe, C. Zaouter, R. Taddei, J. Morse, The Kepler intubation system, Anesth. Analg. 114 (3) (2012) 590–594.

[12] Q. Boehler, D.S. Gage, P. Hofmann, A. Gehring, C. Chautems, D.R. Spahn, P. Biro, B.J. Nelson, REALITI: A robotic endoscope automated via laryngeal imaging for tracheal intubation, IEEE Trans. Med. Robot. Bionics 2 (2) (2020) 157–164.

[13] T. da Veiga, J.H. Chandler, P. Lloyd, G. Pittiglio, N.J. Wilkinson, A.K. Hoshiar, R.A. Harris, P. Valdastri, Challenges of continuum robots in clinical context: A review, Progress Biomed. Eng. 2 (3) (2020) 032003.

[14] X. Wang, Y. Tao, X. Tao, J. Chen, Y. Jin, Z. Shan, J. Tan, Q. Cao, T. Pan, An original design of remote robot-assisted intubation system, Sci. Rep. 8 (1) (2018) 1–9.

[15] Y. Huang, W. Lai, L. Cao, E. Burdet, S.J. Phee, Design and evaluation of a foot-controlled robotic system for endoscopic surgery, IEEE Robot. Autom. Lett. 6 (2) (2021) 2469–2476.

[16] H. Wang, B. Yang, Y. Liu, W. Chen, X. Liang, R. Pfeifer, Visual servoing of soft robot manipulator in constrained environments with an adaptive controller, IEEE/ASME Trans. Mechatronics 22 (1) (2016) 41–50.

[17] E. Rozeboom, J. Ruiter, M. Franken, I. Broeders, Intuitive user interfaces increase efficiency in endoscope tip control, Surg. Endosc. 28 (9) (2014) 2600–2605.

[18] W. Chen, J. Zhou, S.S. Cheng, Y. Lu, F. Zhong, Y. Gao, Y. Wang, L. Xue, M. Tong, Y.H. Liu, Tele-operated oropharyngeal swab (TOOS) RobotEnabled by TSS soft hand for safe and EffectiveCOVID-19 OP sampling, IEEE Trans. Med. Robot. Bionics 3 (4) (2021) 1040–1050.

[19] P. Barba, J. Stramiello, E.K. Funk, F. Richter, M.C. Yip, R.K. Orosco, Remote telesurgery in humans: A systematic review, Surg. Endosc. (2022) 1–7.

[20] F. Chaumette, S. Hutchinson, Visual servo control. I. Basic approaches, IEEE Robot. Autom. Mag. 13 (2006) 82–90.

[21] J.M. Prendergast, G.A. Formosa, M.E. Rentschler, A platform for developing robotic navigation strategies in a deformable, dynamic environment, IEEE Robot. Autom. Lett. 3 (3) (2018) 2670–2677.

[22] A.D. Dragan, S.S. Srinivasa, A policy-blending formalism for shared control, Int. J. Robot. Res. 32 (7) (2013) 790–805.

[23] Z. Li, M. Shahbazi, N. Patel, E.O. Sullivan, R.H. Taylor, Hybrid robot-assisted frameworks for endomicroscopy scanning in retinal surgeries, IEEE Trans. Med. Robot. Bionics 2 (2) (2020) 176–187.

[24] D. Kundrat, A. Schoob, T. Piskon, R. Grässlin, P.J. Schuler, T.K. Hoffmann, L.A. Kahrs, T. Ortmaier, Toward assistive technologies for focus adjustment in teleoperated robotic non-contact laser surgery, IEEE Trans. Med. Robot. Bionics 1 (3) (2019) 145–157.

[25] N. van der Stap, E.D. Rozeboom, H.J. Pullens, F. van der Heijden, I.A.M.J. Broeders, Feasibility of automated target centralization in colonoscopy, Int. J. Comput. Assist. Radiol. Surg. 11 (3) (2016) 457–465.

[26] Y. Li, K.P. Tee, W.L. Chan, R. Yan, Y. Chua, D.K. Limbu, Continuous role adaptation for human–robot shared control, IEEE Trans. Robot. 31 (3) (2015) 672–681.

[27] V. Girbés-Juan, V. Schettino, Y. Demiris, J. Tornero, Haptic and visual feedback assistance for dual-arm robot teleoperation in surface conditioning tasks, IEEE Trans. Haptics 14 (1) (2020) 44–56.

[28] Y. Yang, Z. Jiang, Y. Yang, X. Qi, G. Liu, Safety control method of robot-assisted cataract surgery with virtual fixture and virtual force feedback, J. Intell. Robot. Syst. 97 (8) (2020).

[29] Y. Chen, S. Zhang, Z. Wu, B. Yang, Q. Luo, K. Xu, Review of surgical robotic systems for keyhole and endoscopic procedures: Atate of the art and perspectives, Front. Med. 14 (4) (2020) 382–403.

[30] E. Lopez, L. Zollo, E. Guglielmelli, Teleoperated control based on virtual fixtures for a redundant surgical system, in: 2013 IEEE/RSJ International Conference on Intelligent Robots and Systems, IEEE, 2013, pp. 450–455.

[31] R. Reilink, S. Stramigioli, S. Misra, Image-based flexible endoscope steering, in: 2010 IEEE/RSJ International Conference on Intelligent Robots and Systems, IEEE, 2010, pp. 2339–2344.

[32] W. Jiang, Y. Zhou, C. Wang, L. Peng, Y. Yang, H. Liu, Navigation strategy for robotic soft endoscope intervention, Int. J. Med. Robot. Comput. Assist. Surg. 16 (2) (2020) e2056.

[33] A. O'dwyer, Handbook of PI and PID Controller Tuning Rules, World Scientific, 2009.


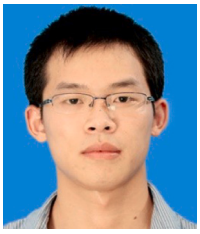

**Zhen Deng** received the M.Sc. degree from the Harbin Institute of Technology, Shenzhen, China, in 2014 and the P.h.D. degree in department of informatik, University of Hamburg, Hamburg, Germany. From 2014 to 2015, he was a research assistant with the Shenzhen Institutes of Advanced Technology, Chinese Academy of Sciences, China. Since 2020, he is working in Fuzhou university, Fujian, China. His current research interests include robot perception and control, and surgical robotics.

**Shengzhan Zhang** received the Bachelor of engineering degree from the Changchun University of Science and Technology, Jilin, China, in 2019, and now he is studying for a master's degree in Mechanics at Fuzhou University, Fujian, China. His current research interest is in robot control and medical robots.

**Yuxin Guo** received the Bachelor of engineering degree from the University of South China in 2021[FF0C?]and now he is studying for a master's degree in Mechanics at Fuzhou University in China. His current research interest is in surgical robots.

**Hongqi Jiang** is currently pursuing B.Eng. in Electronic Engineering at Maynooth International Engineering College, Fuzhou University, China. Her current research interest is surgical robots.

**Xiaochun Zheng** received the Ph.D degrees from China Medical University, China, in 2007. He is a Professor in Shengli Clinical Medical College at Fujian Medical University. He also serves as the director of the Fujian Provincial Key Laboratory of Emergency Medicine, Fujian Provincial Key Laboratory of Critical Medicine, and Fujian Provincial Co-constructed Laboratory of "Belt and Road". He has focus on the research of medical robots, Medical navigation and VR/AR.

**Binwei He** received the Ph.D degrees in mechanical engineering at Xi\' an JiaoTong University, Shanxi, China, in 2003. He is a Professor in the Department of Mechanical Engineering at Fuzhou University. He also serves as the director of the Fujian Intelligent Medical Engineering Research Center and the leader of the Cognitive Robot and Vision Measurement Team. He has been engaged in the theoretical and practical research of robot vision, autonomous navigation and medical surgery operation preview for many years.